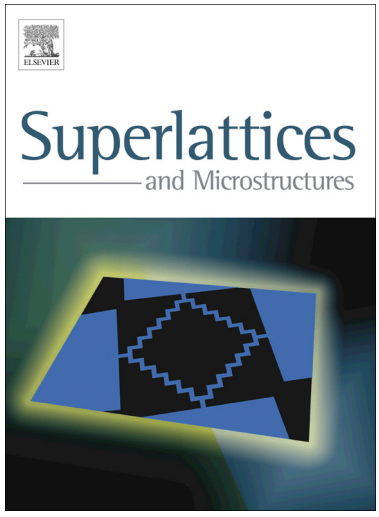

Structural and optical properties of nanoparticles (V, Al) co-doped ZnO synthesized by sol-gel processes

J. El Ghoul, N. Bouguila, S. A. Gómez-Lopera, L. El Mir

PII: S0749-6036(13)00355-8
DOI: http://dx.doi.org/10.1016/j.spmi.2013.10.018
Reference: YSPMI 3056

To appear in: *Superlattices and Microstructures*

Received Date: 21 August 2013
Revised Date: 24 September 2013
Accepted Date: 8 October 2013

Please cite this article as: J. El Ghoul, N. Bouguila, S. A. Gómez-Lopera, L. El Mir, Structural and optical properties of nanoparticles (V, Al) co-doped ZnO synthesized by sol-gel processes, *Superlattices and Microstructures* (2013), doi: http://dx.doi.org/10.1016/j.spmi.2013.10.018

Structural and optical properties of nanoparticles (V, Al) co-doped ZnO synthesized by sol-gel processes

J. El Ghoul [1,*], N. Bouguila [1], S. A. Gómez-Lopera[2] and L. El Mir [1,3]

[1]Laboratoire de Physique des Matériaux et des Nanomatériaux Appliquée à l'Environnement, Faculté des Sciences de Gabès, Cité Erriadh Manara Zrig 6072 Gabès, Tunisie.

[2]Dep. de Fisica Aplicada, Universidad Politécnica de Cartagena (UPCT), Campus Alfonso XIII 30203 Cartagena, Spain.

[3]Al Imam Mohammad Ibn Saud Islamic University (IMSIU), College of Sciences, Departement of Physics, Riyadh 11623, Saudi Arabia.

[*]Corresponding author: Jaber.elghoul@fsg.rnu.tn, ghoultn@yahoo.fr

Highlights

>Elaboration of (V, Al) co-doped ZnO nanoparticles.

>Structural and optical characterizations of these nanoparticles.

>The powder shows an average particle size of 25 nm.

>A strong luminescence band in the visible range is appeared.

Abstract

ZnO, $Zn_{0.9}V_{0.1}O$ and $Zn_{0.89}V_{0.1}Al_{0.01}O$ nanoparticles have been prepared by a sol–gel method and their structural and optical properties have been investigated. The obtained nanopowder was characterized by various techniques such as X-ray diffraction (XRD), transmission electron microscopy (TEM) and photoluminescence (PL) spectroscopy. After thermal treatment at 500 °C in air, the powder of $Zn_{0.89}V_{0.1}Al_{0.01}O$ with an average particle size of 25 nm presents a strong luminescence band in the visible range. The PL band energy position presents a small blue shift with the increase of measurement temperature. Different possible attributions of this emission band will be discussed.

Keywords: ZnO nanocrystal; Optical property; Sol–gel; PL.

1. Introduction

Much effort has been invested in zinc oxide (ZnO), in recent years, for different applications. In fact, due to its direct band gap of 3.37 eV at room temperature, high free-exciton binding energy of about 60 meV, and excilent electrical properties [1-3], ZnO exhibits many significant characteristics. Doped ZnO has emerged as one of the most interesting material for practical applications such as luminescent screens, varistors, lasers, optoelectronic devices and room temperature ferromagnetic materials [4-9]. ZnO photoluminescence has been studied for several decades. Most of the studies represent the PL spectra of ZnO consisting of a sharp exciton related UV luminescence and a defect-related visible emission. The defect-related emissions are located in a wide range of the visible spectrum, such as violet [10], green [11], yellow [12, 13], and orange-red [14–16] emissions. Great efforts have been made to modify and tailor the visible emissions of ZnO by introducing impurities including Al, Mg, Li, V, In, and trioctylamine/trioctylphosphine oxide [17–21]. Recently, Ohashi et al. [22] prepared Li and Al codoped ZnO (LAZO) powders by mixing ZnO powder with aqueous solution of LiCl and $Al(NO)_3$, then drying the mixture and annealing it at 900 °C in oxygen. They observed yellowish-white luminescence from the LAZO powders. Nayak et al. [23] also reported stable, highly intense and yellowish-white luminescence from LAZO nanopowders synthesized via a chemical co-precipitation technique. In most of these studies the synthesis and doping are achieved by a sol-gel process.

Up to now, we have fabricated doped and co-doped ZnO multifunctional materials by sol-gel [24-26] for magnetic and electric properties. We used particularly aluminium which introduces a shallow effective mass like donor state doping. Its solubility range is in the at% range but it might be modified by the co-doping element. For magnetic properties 3d transition metal (TM) like Co, Ni, Mn and V doped ZnO has been performed. In the present paper, we report the effect of vanadium and aluminium as co-doping element of ZnO nanopowder on photoluminescence properties.

2. Experimental details

2. 1. Sample preparation

$Zn_{0.89}V_{0.1}Al_{0.01}O$ nanocrystals were prepared by the sol–gel method using 16 g of zinc acetate dehydrate as precursor in a 112 ml of methanol. After 10 min magnetic stirring at room temperature, 0.628 g of ammonium metavanadate corresponding to [V]/[Zn] = 0.10 and an adequate quantity of aluminium nitrate-9-hydrate corresponding to [Al]/[Zn] ratios of 0.010 were added. After an additional 15 min magnetic stirring, the solution was placed in an autoclave and dried under supercritical conditions of ethyl alcohol (EtOH). The obtained powder was then heated in a furnace at 500 °C for 2 hours in air.

2. 2. Characterisation techniques.

The crystalline structure and phase purity of the aerogel after thermal treatment were investigated by X-ray diffraction using the CuKα radiation (λ=1.5418 Å) of a Bruker D5005 diffractometer. The aerogel powders were also characterized using a JEM-200CX transmission electron microscope (TEM). The specimens for TEM were prepared by putting the as-grown products in ethyl alcohol and immersing them in an ultrasonic bath for 15 min, then dropping a few drops of the resulting suspension containing the synthesized materials onto TEM grid. For PL measurements, the 450 Xenon lamp was used as an excitation source. The emitted light from the sample, collected by an optical fibre on the same side as the excitation, was analysed with a Jobin-Yvon Spectrometer HR460 and a multichannel CCD detector (2000 pixels). The PLE measurements were performed on Jobin-Yvon Fluorolog 3-2 spectrometer. The emission spectra were corrected for the spectral response of the excitation source. The low temperature experiments were carried out in a Janis VPF-600 Dewar with variable temperature controlled between 78 K and 300 K.

3. Results and discussion

Fig. 1 shows typical XRD spectra of the aerogel powders of ZnO, $Zn_{0.9}V_{0.1}O$ and $Zn_{0.89}V_{0.1}Al_{0.01}O$. In the case of undoped ZnO, we noticed the appearance of nine pronounced diffraction peaks at 2θ = 31.82°, 34.61°, 36.36°, 47.55°, 56.73°, 62.88°, 66.34°, 68.08° and 69.19° which can be attributed to the (100), (002), (101), (102) (110), (103), (200), (112) and (201) planes of ZnO, respectively [27]. After doping of ZnO and thermal treatment, in addition to the peaks corresponding to ZnO, four secondary additional phases were detected

which can be attributed to $VO_2(120)$, $V_2O_3(012)$, $V_2O_5(101)$ and $Zn_3(VO_4)$ in the case of vanadium doping [27, 28]. By against, we have not noticed the appearance of peaks corresponding to aluminum doping. Due to the small size of the crystallites in the aerogel, the diffraction lines are broadened and are further found to depend on the Miller indices of the corresponding sets of crystal planes. The average grain size can be calculated using the Debye-Sherrer equation [29]:

$$G = 0.9\lambda / B\cos\theta_B \qquad (1)$$

where λ is the X-ray wavelength (1. 5418 Å), θ_B is the maximum of the Bragg diffraction peak and B is the linewidth at half maximum. After a correction for the instrumental broadening, an average value of the basal diameter of the cylinder-shape crystallites is found to be 15-22 nm, whereas the height of the crystallites is 22-30 nm. From the symmetric peaks, we find that the lattice parameter c of $Zn_{0.89}V_{0.1}Al_{0.01}O$ (c = 5.191 Å) is smaller than the value c of undoped ZnO (c = 5.210), which is close to the value of conventional nanosized crystallites {c-lattice from crystallographic data: ICSD reference number: 67848–1993 (5.2151 Å) and 67454–1989 (5.2071 Å)}. This reduction in lattice parameter may be due to a diminution in size of the nanoparticles after doping [28].

The SEM images in Fig. 2 show that the grains are formed in hexagonal structure. At first glance, it is clear that the grain size is nanometric for the three samples. Fig. 3 shows the TEM images of representative particles of these three samples well as the HRTEM image of ZnO and EDX analyzes of doped samples. The morphologies of all the samples are found to be nearly spherical in nature with the diameters ranging from 19 to 28 nm. It clearly shows that the average particle size of these samples is nanoscale and it is in accordance with the results of the XRD. The HRTEM image clearly showed that the measured distance between the planes of the fringes is 0.26 nm (Fig. 3 a), which is corresponding to the (002) planes of the wurtzite ZnO. The EDX spectra of the doped samples showed signals directly related to the dopants. Zn and O appeared as the main components with low levels of V and Al (Fig. 3 b, c). This confirmed the formation of Al and V co-doped ZnO.

The optical properties of the material are shown in Fig. 3. The spectra are characterized by an intense fundamental absorption due to nanoparticles ZnO in the region between 300 and 400 nm (Fig. 4a). There is a red shift in the absorption edge for $Zn_{0.89}V_{0.1}Al_{0.01}O$ that can be attributed to the presence of V and Al in the ZnO.

The reflectance spectral data were converted to the Kubelka–Munk function, F(R) by applying the equation:

$$F(R) = \frac{(1-R)^2}{2R} \qquad (2)$$

The Kubelka–Munk function can be transformed to a Tauc plot-a plot of $[F(R).h\nu]^n$ versus hv. A direct band gap semiconductor gives a linear Tauc region just above the optical absorption edge with n=2, whilst an indirect semiconductor gives a linear region with n=0.5 [30]. A direct band gap semiconductor was assumed for these samples since a linear region just above the gap edges was observed with n=2.

Plotting $[F(R).h\nu]^2$ as a function of photon energy, and extrapolating the linear portion of the curve to absorption equal to zero as shown in Fig. 4b, gives the values of the direct band gap (Eg) to be 3.19 eV, 3.14 eV, and 3.04 eV for the samples of ZnO, $Zn_{0.9}V_{0.1}O$, and $Zn_{0.89}V_{0.1}Al_{0.01}O$, respectively. Based on the presence of VO groups confirmed by XRD, we expect that the small direct band gap of the VO groups such as V_2O_5 (2.3 eV) [31] may be responsible for the decrease of the band gap in our V-doped ZnO samples.

The PL study was carried out for evaluate the quality and evolution of the emission for two different wavelengths depending on the temperature of measurement. Fig. 5 shows the PL spectra of the of ZnO, $Zn_{0.9}V_{0.1}O$ and $Zn_{0.89}V_{0.1}Al_{0.01}O$ nanopowder after heat treatment in an oven for 2 hours at 500 ° C in air excited by 325 nm at room temperature. The undoprd ZnO annealed in air exhibit a strong ultraviolet emission peak at 380 nm, which corresponds to the near band edge peak that is responsible for the recombination of free ZnO excitons [32]. Generally, the intensity ratio between the ultraviolet emission band and the deep-level emission band is regarded as an indicator of the crystallinity of ZnO materials. In the case of ZnO doped, the PL spectra consist of a broad emission band located in the visible range of the green-yellow-red. We showed in our works that the luminescence band in the case of metal transition elements (MT) doped ZnO is attributed to the effects of doping [24, 19, 33]. Other emissions in visible range were observed but the centres responsible of these emission bands and the related recombination mechanisms are not still understood and call further investigations.

The origins of the emission bands in ZnO, are yet highly controversial and many attributions have been proposed [34-36]. Generally, ZnO exhibits two visible bands centred at 510–540 nm (green emission) and 600–640 nm (yellow emission), attributed to oxygen vacancy (V_O^+) [34] and oxygen interstitial (O_i^-) [35], respectively. Jin et al. [34] reported a violet emission at 420 nm and attributed it to a transition between radiative defects level and the valence band. These radiative defects are related to the interface traps existing at the grain. Jeong et al. [35] believed that the Zn vacancies V_{Zn} are responsible for the violet emission at

401 nm wavelength. Fu et al. [36] found a violet emission located at 392 nm in ZnO films on silicon substrate, they thought that this emission originated from the electron transition from the conduction band to the valence band. It has been suggested that the green emission is associated to oxygen deficiency, while the orange-red emission is associated to oxygen excess [37].

Fig. 6 (a) and (b) illustrates the temperature dependence of the $Zn_{0.89}V_{0.1}Al_{0.01}O$ nanopowder PL spectra, for two wavelength excitations (325 and 371nm). The PL band intensity increases with decreasing temperature. However, the blue shift is more pronounced under 325 nm excitation wavelength than that under 371 nm. The two band intensities increase with the increase of temperature. To the best of our knowledge, this blue shift behaviour of these emission bands with temperature measurement had never been reported.

Concerning our two emission bands, the fact that: (i) each one is observed under different excitation energy and (ii) they show a different behaviour with temperature variation (the energy shift is more important for the emission band observed under 330nm excitation wavelength than that observed under excitation at 371 nm wavelength) are a good indication that their origins are different. The nature of the centres responsible of these emission bands and the related recombination mechanisms are not still understood and call for further investigations. But we can conclude that doping ZnO with Al leads to green emission [38], while V-doping causes yellow emission [27, 28].

One suggested that emission located to about 670 nm is in report with the competition between V_o^+ and O_i^-. When impurity Al or V replaces Zn in the lattice, excess oxygen will be introduced as interstitial oxygen due to charge equilibrium [24].

In order to get further information about the recombination mechanisms responsible of the emission bands around 550, 630, 640 and 760 nm, photoluminescence excitation (PLE) measurements were performed (Fig 7). These wavelengths were chosen in order to analyse the different emissions. In fact, for the emission at 600 nm, we studied the wavelength of analysis at 550 nm corresponding to the short wavelength limit, and for the emission at 700 nm, we studied the wavelength of analysis at 760 nm corresponding to the high wavelength limit, and two other wavelengths in the middle at 630 and 640 nm were used in order to see the contribution of the different centres of emission in this region.

The PLE spectrum relative to defect emission presents a strong band at 371 nm observed at 78 K, this band shifts towards the bass energy at 300 K, this behaviour and this position proves the contribution of ZnO nanoparticles.

4. Conclusion

(V, Al) co-doped zinc oxide nanoparticles were synthesized by sol-gel method. The protocol of elaboration is based on slow hydrolysis of the precursor using an esterification reaction, followed by a supercritical drying in EtOH. The X-ray diffraction and TEM analysis indicated the presence of nanocrystallites aggregated in different shape particles. Kubelka–Munk Tauc plots showed decrease of the band gap in our doped ZnO samples. PL spectra of the nanopowder showed strong yellow-red luminescence band. From analysis of the results, it can be concluded that the contents of defect complexes involved by oxygen excess which introduced as interstitial oxygen due to charge equilibrium, associated with the presence of dopants in the powder was responsible of this luminescence band. The formation mechanism and the chemical nature of this defect complex will be the subject of our future intensive study.

References

[1] V. Musat, A. M. Rego, R. Monteiro, E. Forttunato, Thin Solid Films 516 (2008) 1512.

[2] T. Minami, S. Ida, T. Yao, Mater. Sci. Eng. B 75 (2000)190.

[3] L. El Mir, Z. Ben Ayadi, H. Rahmouni, J. El Ghoul, K. Djessas, H. J. von Bardeleben; Thin Solid Films 517 (2009) 6007.

[4] L. Grigorjeva, D. Millers, K. Smits, C. Monty, J. Kouam, L. El Mir, Solid State Phenomena 128 (2007) 128.

[5] L. Yan, C. K. Ong, X. S. Rao, J. Appl. Phys. 96 (2004) 508.

[6] D. H. Kim, S.I. Woo, S.H. Moon, H.D. Kim, B.Y. Kim, J. H. Cho, Y.G. Joh, E.C. Kim, Solid State Commu. 136 (2005) 554.

[7] S. Choopun, R.D.Vispute, W. Noch, A. Balasamo, R.P. Sharma, T. Venkatesan, A. Lliadies, D.C. Look, Appl. Phys. Lett. 75 (1999) 3947.

[8] K. Ueda, H. Tabata, T. Kawai, Appl. Phys. Lett. 79 (2001) 988.

[9] P. Nunes, E. Fortunadeo, R. Martins, Thin Solid Films 383 (2001) 277.

[10] B. J. Jin, S . Im, S. Y. Lee, Thin Solid Films 366 (2000) 107.

[11] K. Vanheusden, W. L. Warren, C. H. Seager, D. R. Tallant, J. A. Voigt, B. E. Gnade, J Appl Phys 79 (1996) 7983.

[12] L. E. Greene, M. Law, J. Goldberger, F. Kim, J. C. Johnson, Y. Zhang, R. J. Saykally, and P. Yang, Angew. Chem. Int. Ed 42 (2003) 3031.

[13] Y. W. Heo, D. P. Norton, S. J. Pearton, J Appl Phys 98 (2005) 1.

[14] S. A. Studenikin, N. Golego, M. Cocivera, J Appl Phys 84 (1998) 2287.

[15] X. Liu, X. Wu, H. Cao, R. P. H. Chang, J Appl Phys 95 (2004) 3141.

[16] M. Wang, E. J. Kim, J. S. Chung, E.W. Shin, S. H. Hahn, K. E. Lee, C. Park, Phys Status Solidi A 203 (2006) 2418.

[17] L. J. Li, H. Deng, L. P. Dai, J. J. Chen, Q. L. Yuan, Y. Li, Mater Res Bull 43 (2008) 1456.

[18] S. Fujihara, Y. Ogawa, A..Kasai, Chem Mater 16 (2004) 2965.

[19] L. El Mir, J. El Ghoul, S. Alaya, M. Ben Salem, C. Barthou, H.J. von Bardeleben. Physica B 403 (2008) 1770.

[20] J. Y. Lee, B. R. Jang, J. H. Lee, H. S. Kim, H. K. Cho, J. Y. Moon, W. J. Lee, J. W. Baek, Thin Solid Films 517 (2009) 4086.

[21] Y. Gong, T. Andelman, G.F. Neumark, S. O'Brien, I.L. Kuskovsky, Nanoscale Res Lett 2 (2007) 297.

[22] N. Ohashi, N. Ebisawa, T. Sekiguchi, I. Sakaguchi, Y. Wada, T. Takenaka, H. Haneda, Appl Phys Lett 86 (2005) 1.

[23] J. Nayak, S. Kimura, S. Nozaki, H. Ono, K. Uchida, Superlattices and Microstrures 42 (2007) 438.

[24] L. El Mir, Z. Ben Ayadi, M. Saadoun, H. J. von Bardeleben, K. Djessas, A. Zeinert, Phys. Stat. Sol. (a) 204 (10) (2007) 3266.

[25] L. El Mir, Z. Ben Ayadi, M. Saadoun, K. Djessas, H. J. von Bardeleben, S. Alaya. Appl. Surf. Sci. 254 (2007) 570.

[26] L. El Mir, F. Ghribi, Z. Ben Ayadi, K. Djessas, M. Cubukcu, H. J. von Bardeleben; Thin Solid Films 519 (2011) 5787.

[27] J. El Ghoul, C. Barthou and L. El Mir, Superlattices and Microstructures, 51 (2012) 942.

[28] J. El Ghoul, C. Barthou and L. El Mir, Physica E Low-dimensional Systems and Nanostructures, 44 (2012) 1910.

[29] L. Wang, L. Meng, V. Teixeira, S. Song, Z. Xu, X. Xu; Thin Solid Films 517 (2009) 3721.

[30] A. T. Kuvarega, R.W. M. Krause, B. B. Mamba, J. Phys. Chem C, 115 (2011) 22110.

[31] S. F. Cogan, N. M. Nguyen, S. J. Perrotti, R. D. Rauh, J. Appl. Phys. 66 (1989) 1333.

[32] Y.C. Kong, D.P. Yu, B. Zhang, et al, Appl. Phys. Lett. 78 (2001) 407

[33] J. El Ghoul, C. Barthou, M. Saadoun, L. El Mir, Physica B 405 (2010) 597

[34] B. J. Jin, S. Im, S. Y. Lee, Thin Solid Films 366 (2000) 107.

[35] S. H. Jeong, B. S. Kim, B. T. Lee, Appl. Phys. Lett. 82 (2003) 2625.

[36] Z. X. Fu, C. X. Guo, B. X. Lin, G. H. Liao, Chim. Phys. Lett. 15 (1998) 457.

[37] A. Teke, U. Ozgur, S. Dogan, X. Gu, H. Morkoç, B. Nemeth, J. Mause, H.O. Everitt, Phys. Rev; B 70 (2004) 195207.

[38] M. Wang, K. E. Lee, S. H. Hahn, E. J. Kim, S. Kim, J. S. Chung, E. W. Shin, C. Park, Mater Lett 61 (2007) 1118.

Figure captions

Figure 1. X-ray diffraction spectra of ZnO (a), $Zn_{0.9}V_{0.1}O$ (b) and $Zn_{0.89}V_{0.1}Al_{0.01}O$ (c) nanoparticules.

Figure 2. Typical SEM micrograph of (a) ZnO, (b) V-doped ZnO and (c) (V, Al) co-doped ZnO nanoparticles.

Figure 3. HR-TEM images and EDX analysis of (a) ZnO (b) $Zn_{0.9}V_{0.1}O$ (c) $Zn_{0.89}V_{0.1}Al_{0.01}O$ nanoparticles.

Figure 4 a. Absorbance and reflectance spectra of ZnO, $Zn_{0.9}V_{0.1}O$ and $Zn_{0.89}V_{0.1}Al_{0.01}O$ nanoparticules.

Figure 4 b. Kubelka–Munk Tauc plots of ZnO, $Zn_{0.9}V_{0.1}O$ and $Zn_{0.89}V_{0.1}Al_{0.01}O$ nanoparticules.

Figure 5. PL spectra of ZnO, $Zn_{0.9}V_{0.1}O$ and $Zn_{0.89}V_{0.1}Al_{0.01}O$ nanoparticules at 78 K.

Figure 6. PL spectra of $Zn_{0.89}V_{0.1}Al_{0.01}O$ nanoparticules at different temperature measurements for λ_{exc}=325 nm and λ_{exc}=371 nm.

Figure 7. PLE spectra of $Zn_{0.89}V_{0.1}Al_{0.01}O$ nanoparticles detected at 550nm, 640 nm, 760nm and 630nm.

Fig. 1

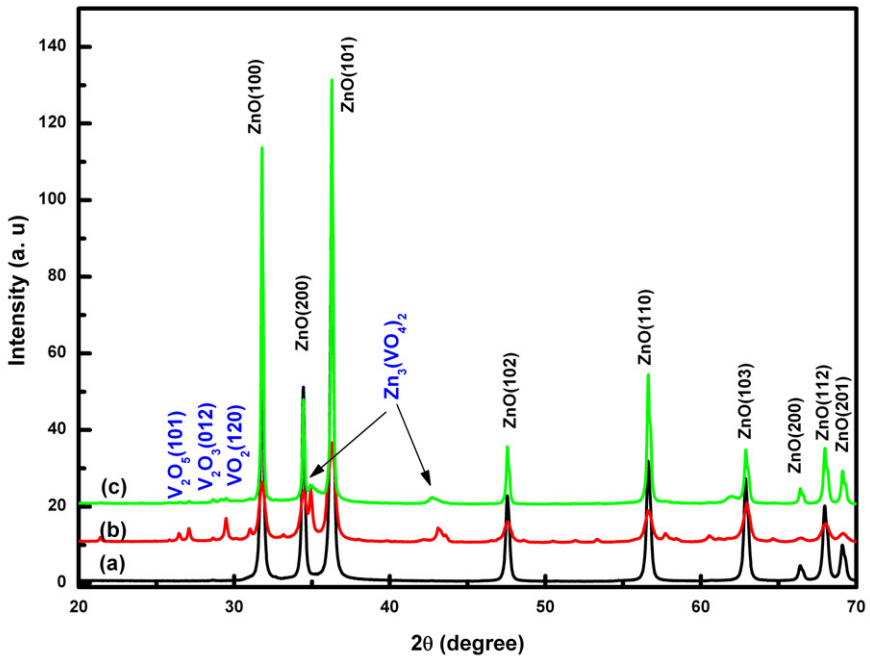

Fig. 2

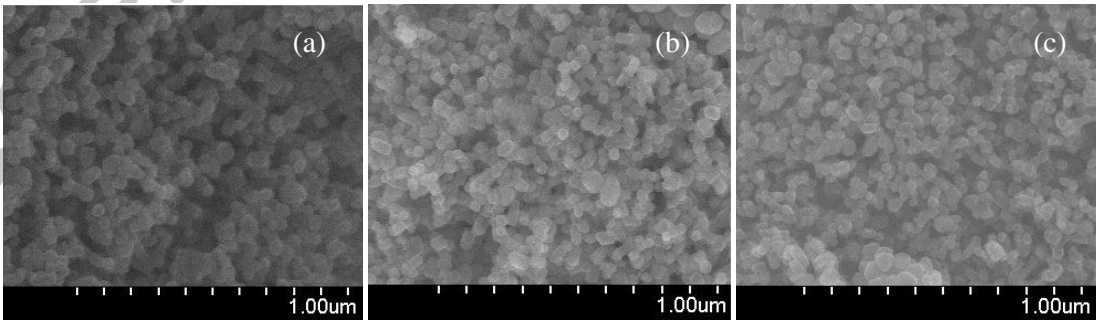

Fig. 3

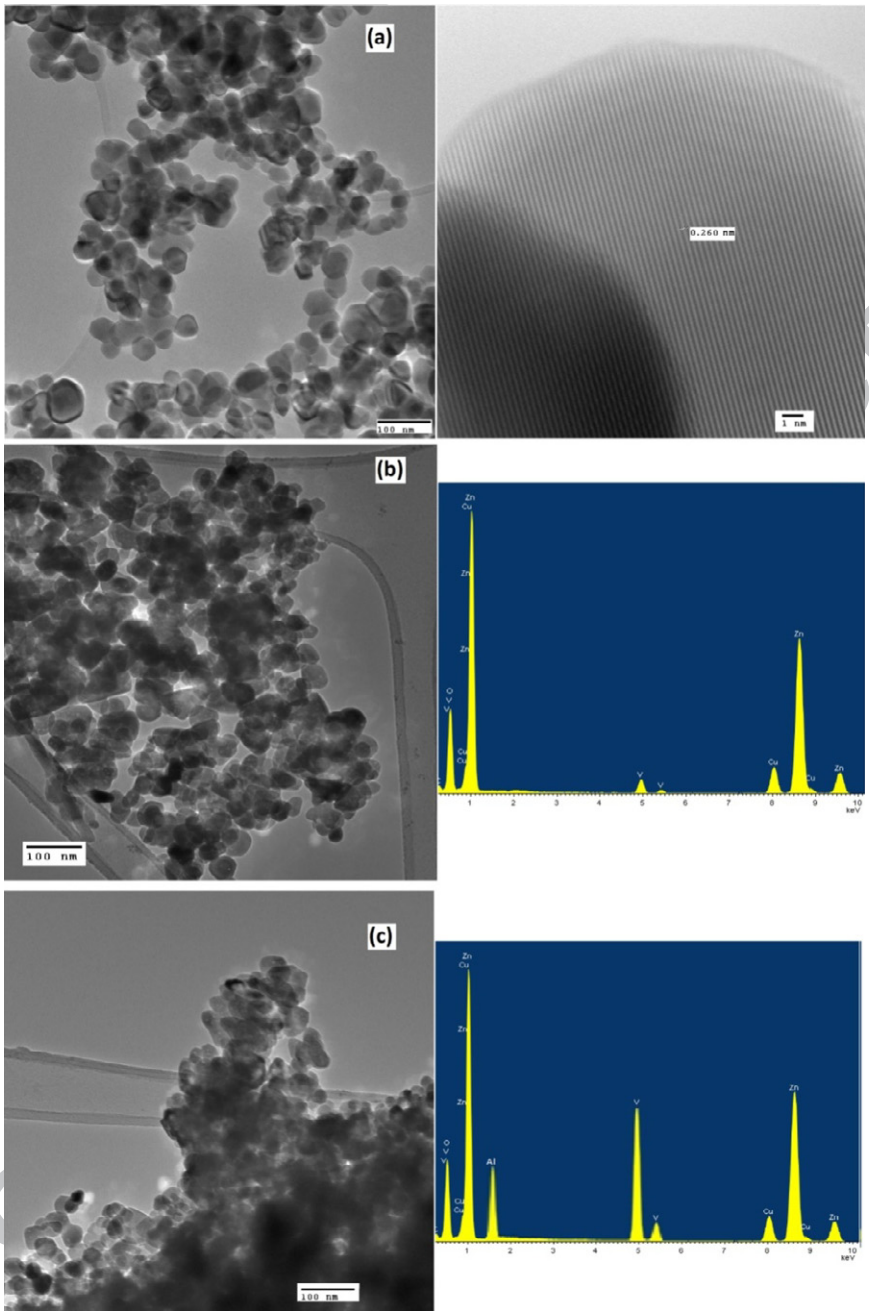
(a)
100 nm
0.260 nm
1 nm
(b)
100 nm
Zn
Cu
Zn
Zn
V
O
V
Cu
Cu
V
V
Cu
Cu
Zn
keV
(c)
100 nm
Zn
Cu
Zn
Zn
V
O
V
Al
Cu
Cu
V
V
Cu
Cu
Zn
keV

Fig. 4

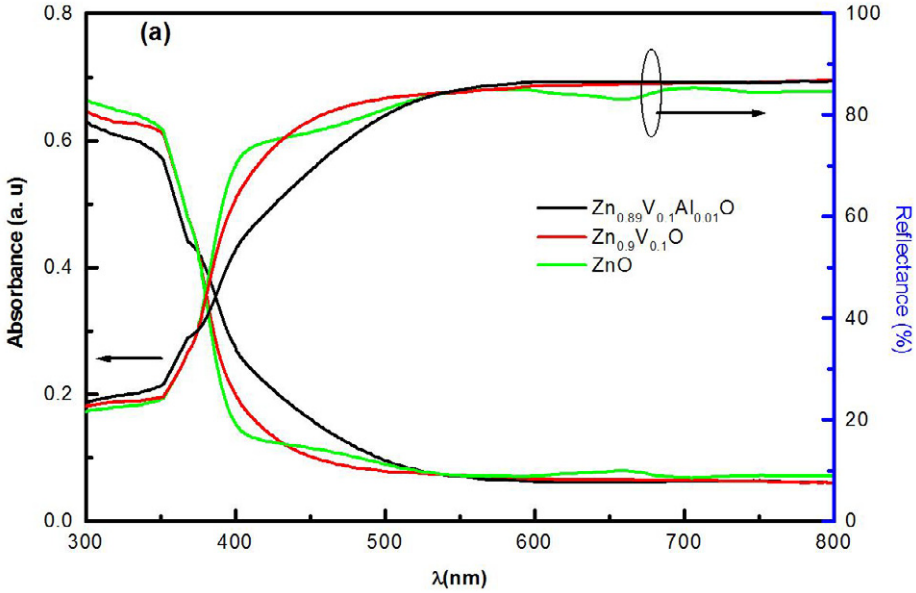
(a)
Absorbance (a. u)
Reflectance (%)
λ(nm)
$Zn_{0.89}V_{0.1}Al_{0.01}O$
$Zn_{0.9}V_{0.1}O$
ZnO

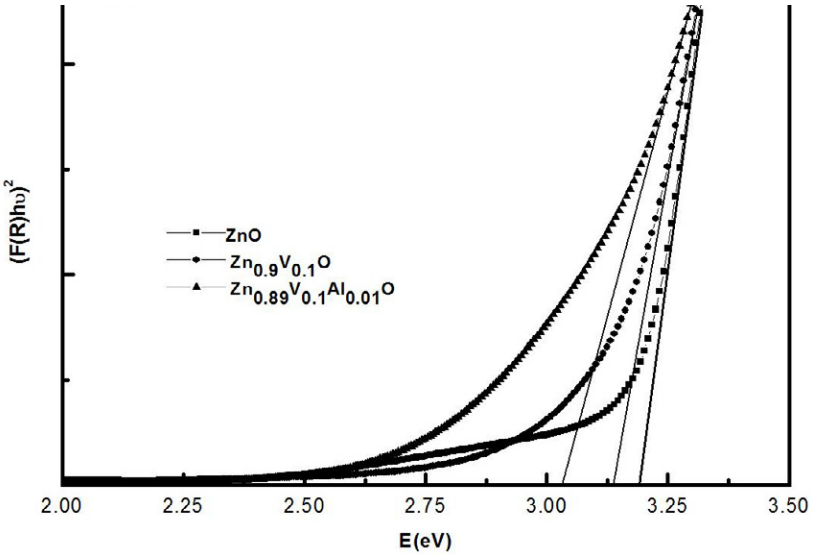
$(F(R)h\upsilon)^2$
E(eV)
ZnO
$Zn_{0.9}V_{0.1}O$
$Zn_{0.89}V_{0.1}Al_{0.01}O$

Fig. 5

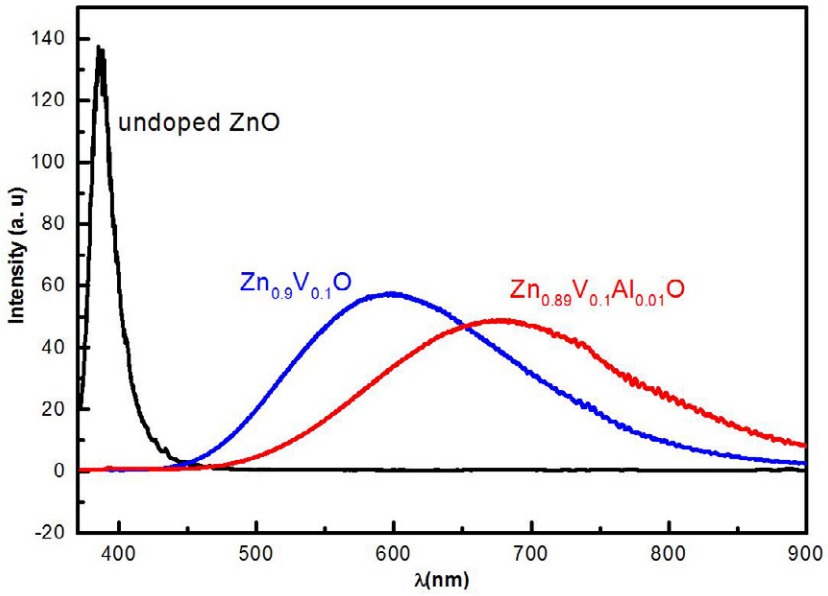

Fig. 6

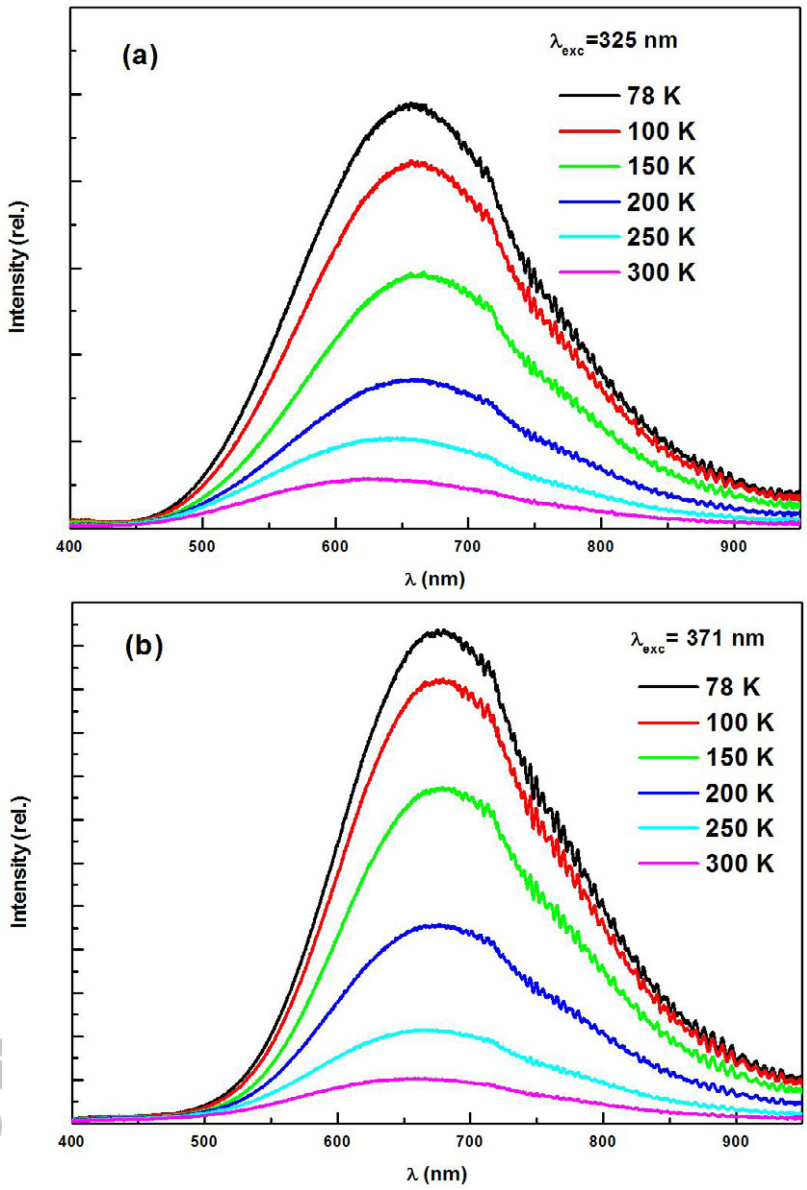

Fig. 7